Low loss germanium-on-silicon waveguides for integrated mid-infrared photonics

R. W. Millar, K. Gallacher, U. Griskeviciute, L. Baldassarre, M. Sorel, et al.

R. W. Millar, K. Gallacher, U. Griskeviciute, L. Baldassarre, M. Sorel, M. Ortolani, D. J. Paul, "Low loss germanium-on-silicon waveguides for integrated mid-infrared photonics," Proc. SPIE 10923, Silicon Photonics XIV, 109230S (4 March 2019); doi: 10.1117/12.2510009

SPIE.

Event: SPIE OPTO, 2019, San Francisco, California, United States

Low Loss Germanium-on-Silicon waveguides for integrated Mid-infrared Photonics

R. W. Millar[1,3], K. Gallacher[1,3], U. Griskeviciute[1], L. Baldassarre[2], M. Sorel[1], M. Ortolani[2] and D. J. Paul[1,*]

[1]University of Glasgow, School of Engineering, Rankine Building, Oakfield Avenue, Glasgow, G12 8LT, UK
[2]Dipartimento di Fisica, Universita di Roma La Sapienza, Piazzale Aldo Moro 5, I-00185 Roma, Italy
[3]*These authors contributed equally to the work.*

ABSTRACT

Low loss Ge-on-Si waveguides are demonstrated in the 8 – 14 μm atmospheric transmission window, a technology that will enable detection and sensing of unique molecular vibrations. Such a low cost platform would have applications in key markets such as pollution monitoring, explosives detection and point of care diagnostics. Rib-waveguides are fabricated using electron beam lithography and dry etching. The waveguides propagation losses are characterized using the Fabry-Perot technique, and are found to be below 5 dB/cm across the measurement range of 7.5 to 11 μm wavelength, reaching as low as ~ 1 dB/cm. The contribution to the losses are analyzed using the experimentally measured Si substrate losses, and the calculated scattering losses from an analytical model. The results verify the feasibility of the Ge-on-Si platform for integrated mid-infrared photonics and sensing.

Keywords: mid-infrared, germanium, waveguide

1. INTRODUCTION

Germanium-on-Si waveguides have been viewed as an attractive platform for integrated mid-infrared (MIR) photonics for a number of years [1]. The primary motivation for such a platform is for MIR sensing in the molecular fingerprint regime, defined as 6.7 – 20 μm wavelength, where label free detection is possible due to the unique absorption spectra of a number of molecules. Integrated sensors could therefore be realized using the low cost Ge-on-Si platform, with potential applications including explosives detection [2], as well as pollution monitoring and point of care diagnostics using breath bio-markers [3]. The two major spectral regions of interest in the mid-infrared (MIR) for applications are the 3 to 5 μm, and 8 to 14 μm wavelength, which are low atmospheric absorption windows [3]. The 3 to 5 μm gas detection window has a wide range of gas detectors available with both sources and photodetectors for CO_2, O_2, CH_4 and many other small molecules [4]. The 8 to 14 μm window is more important for larger molecules, particularly as many biological and chemical molecules have unique molecular absorption inside this window, including the majority of explosives [5], chemical weapons [6], biological markers and pollutants.

In recent years there has been a number of demonstrations of Si based, active and passive photonic components operating in the MIR, including Ge plasmonics [7,8], SiGe quantum well [9] and quantum dot [10] detectors, and GeSn light sources [11-13]. In terms of waveguides, while the Silicon-on-insulator platform has become established at telecoms wavelengths, strong absorption from silicon dioxide > 3.6 μm wavelength limits the use of the platform into the mid-infrared [14]. Silicon-on-nothing platforms have been investigated by removing the buried oxide layer, and have demonstrated low losses of ~ 3 dB/cm up to 7.67 μm wavelength [15]. Such platforms, however, require added complexity and could be prone to mechanical stability issues. As a result, a number of alternative material platforms have been investigated for integrated MIR photonics. Alloying Ge with Si can extend the transparency of the material, and provide sufficient index contrast with the Si for SiGe-on-Si waveguides, where low losses and even supercontinuum generation has been demonstrated [16]. High Ge content SiGe layers can also be grown on graded SiGe buffers on Si substrates, where broadband passive components [17] and low loss waveguides [18] have been demonstrated up to 8.5 μm wavelength. Germanium is an ideal MIR material, with high transparency up to 16 μm wavelength, and low costs due to Si growth and fabrication compatibility. Furthermore, Ge has a larger $\chi^{(3)}$ coefficient than Si, and is therefore well suited to non-linear processes [19,20]. Previously, there have been a number of demonstrations of Ge-on-Si waveguides with low losses shown at wavelengths of 3.8 [21] and 5.8 μm [22] as well as a number of components such as modulators [23], grating couplers [24] and ring resonators [25]. Recently, Ge-on-nothing waveguides have been shown

Silicon Photonics XIV, edited by Graham T. Reed, Andrew P. Knights, Proc. of SPIE Vol. 10923
109230S · © 2019 SPIE · CCC code: 0277-786X/19/$18 · doi: 10.1117/12.2510009

with low loss up to 7.67 µm [26], and Ge-on-Si waveguides were demonstrated up to 8.5 µm wavelength [27], which exhibited relatively high propagation losses of ~ 20 dB/cm. The loss mechanism was not verified but it is likely that the losses were in part due to free carrier losses from background doping.

In this work, we investigate Ge-on-Si waveguides up to 11 µm wavelength, enabling us to experimentally verify the contribution to the waveguide losses from the Si substrate (lower cladding) for the first time. Losses below 5 dB/cm across the full measurement range (7.5 to 11 µm) are found in both transverse electric (TE) and transverse magnetic (TM) polarization, reaching as low as ~ 1 dB/cm at ~ 10 µm wavelength. These record losses are believed to be the lowest measured for an integrated dielectric waveguide on chip at longer wavelengths than 10 µm, and therefore confirm the feasibility of the platform for integrated waveguide sensing in the 8- 14 µm atmospheric transmission window.

2. GROWTH

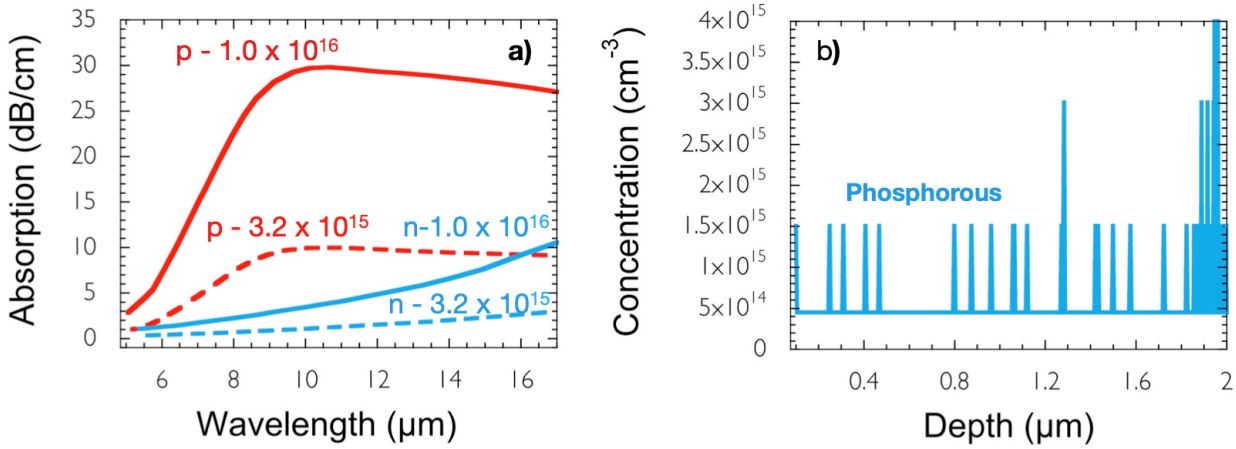

Figure 1: a) Free carrier absorption in p and n-type Ge using data from [30-32], for two doping conenctrations (cm^{-3}). b) Secondary Ion Mass Spectrometer data for phosphorous in 2 µm thick Ge grown on Si.

Germanium epitaxial layers of 2 µm thickness were grown at IQE Silicon by reduced-pressure chemical-vapour-deposition (RP-CVD), on 150 mm diameter Si (001) substrates. The Si subtrates were grown by the Czochralski (Cz) method, and therefore have oxygen impurities on the order of 10^{18} cm^{-3} [28]. The Si substrate resistivity of 10 – 20 ohm-cm corresponds to a phosphorous doping concentration of approximately 5 x 10^{14} cm^{-3}. The Ge epitaxial layer was grown using the two-temperature technique [29] and subsequently cyclically annealed in order to minimize the threading dislocation density to < 10^{7} cm^{-2} at the top surface. In order to eliminate a potential source of waveguide losses, it was ensured that the background doping was minimized. At MIR wavelengths even a moderate background doping can cause significant free carrier loss. In Ge, excess hole densities cause significantly higher absorption than electrons. This is due to the fact that holes populating the valence band can allow strong inter-valence band transitions to take place that are direct in k-space. This is in contrast to electrons in the conduction band, which require phonon scattering, in a second order process, to conserve momentum. As a result, while intrinsic Ge growth is desirable, it is preferable to have an n-type background doping compared to a p-type background. This can be illustrated in Fig 1a), which shows the modeled free carrier losses, calibrated from experimental data, using data from [30-32]. The data has been plotted in dB/cm, which is equivalent to waveguide propagation in a Ge core where the optical mode is fully contained in the Ge. In order to avoid a p-type background, an n-type (phosphorous) doped Si wafer was chosen so that any potential segregation would lead to n-type doping in the Ge. Furthermore, an RP-CVD reactor was used where only phosphorous had been used as a dopant source. The grown material was confirmed to be n-type by using the 'hot probe technique' [33], and the doping density was confirmed using secondary ion mass spectroscopy, in a system with sensitivity to phosphorous down to 5 x 10^{14} cm^{-3}. As shown in Fig 1b), the doping density is indeed at the noise floor, with the presence of peaks attributed to noise from the electron multiplier. These sporadic counts appear as significant peaks in concentration due to the small binning of data in the z-direction, i.e. if all electron multiplier counts were averaged over the total Ge thickness it would be almost indistinguishable from the noise floor. It can therefore be assumed that free carrier losses do not contribute significantly to the waveguide propagation losses.

3. FABRICATION

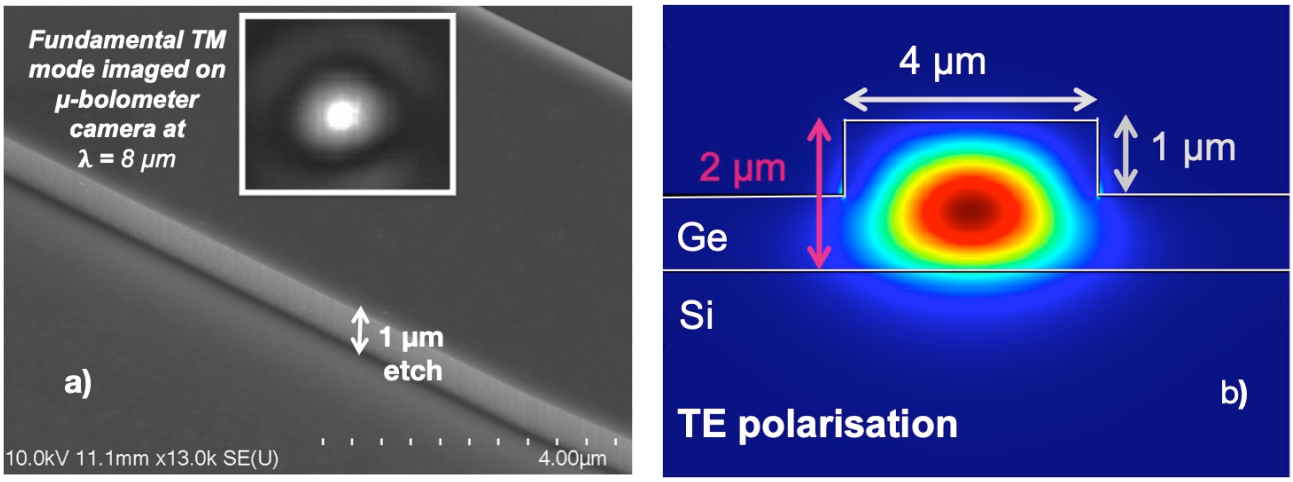

Figure 2: a) A scanning electron microscope image of an etched Ge-on-Si rib waveguide. Inset shows the optical mode imaged on a μ-bolometer camera. b) Simulated mode profile of the fundamental transverse electric mode at 8 μm wavelength, in a Ge rib waveguide.

Serpentine waveguides of 4 μm width were patterned using electron beam lithography, Fig. 2a). To minimize line edge roughness a 'bulk and sleeve' technique was used, which allows the outer edge of the waveguides to be written using a smaller diameter electron beam, with a larger beam used for the waveguide center. This minimizes the line edge roughness while allowing a fast patterning time. A width of 4 μm was chosen to allow for single mode operation, Fig. 2b), across the measurement range, which is a requirement for the Fabry-Perot method for measuring loss. The waveguides were etched using a mixed SF_6 and C_4F_8 etch to a depth of 1 μm to form rib waveguides. As shown in Fig. 2a) this results in vertical sidewalls that appear smooth by scanning electron microscopy. The waveguide width is tapered adiabatically up to 12.5 μm wide at the facet to increase optical coupling.

4. CHARACTERISATION

The waveguide losses were measured using a Daylight Solutions Quantum Cascade Laser (QCL) package, containing 4 separate QCL chips, covering the wavelength range of 7.5 to 11.5 μm. The laser emission is coupled to and from the waveguides via a pair of ZnSe lens with a numerical aperture of 0.25. Waveguide aligned is achieved with a Xenix Gobi amorphous Si μ-bolometer camera, and losses were measured using a DLaTGS detector. The setup is shown in Fig. 3. The source was modulated with an optical chopper and the output of the detector was input to a LabView controlled lock-in amplifier, in order to improve signal-to-noise and remove the effects of ambient blackbody radiation in the room. The QCL package cannot be continuously tuned without mode hopping, so in order to observe Fabry-Perot fringes the sample temperature is tuned via a resistive heater, which modifies the material refractive index via the thermo-optic effect [34]. A downside of this measurement technique is that there is thermal expansion of the stage, which causes the waveguide alignment to drift. Serpentine waveguides were chosen to increase the optical path length (cavity length), therefore increasing the number of fringes observed for a given temperature change, and increasing the number of fringes observed before significant misalignment of the waveguide to the objectives. A bending radius of 500 μm was chosen to ensure bending losses are negligible. The waveguide propagation losses are then calculated using the standard fringe contrast expression [35], which requires knowledge of the facet reflectivity. Here, the facet Fresnel reflectivity was calculated using the effective index of the propagating mode, as modeled by the Finite Difference Eigenmode method. In practice, the waveguide facets will be imperfect, and may have reduced reflectivity compared to the ideal scenario, however, the assumption of ideal facets would only serve to overestimate the propagation loss.

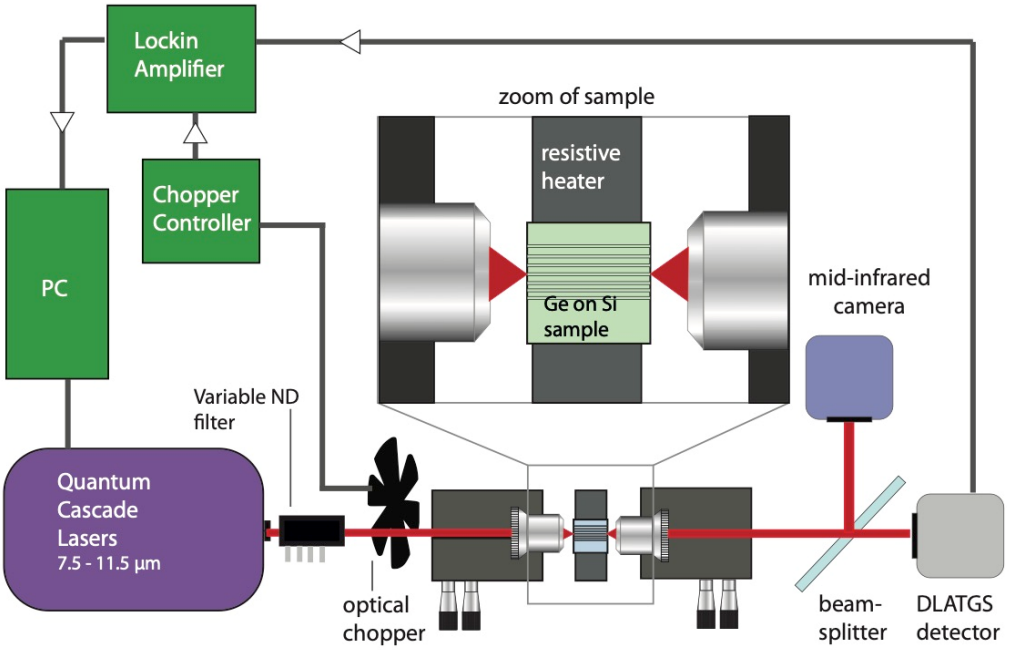

Figure 3: Schematic of the setup for optical loss measurements of the Ge-on-Si waveguides.

5. RESULTS

The measured waveguide losses are shown in Fig. 4. A solid line has been added to link the data points as a guide for the eye. Across the measurement range, propagation losses are below 5 dB/cm for both TM and TE polarizations. Notably, there is a rise in the losses for both TE and TM modes at ~ 9 µm wavelength. There is a known absorption peak at 9 µm wavelength in Cz Si substrates, due to interstitial oxygen impurities [28]. To check for consistency with this mechanism, the Si substrate losses were experimentally measured.

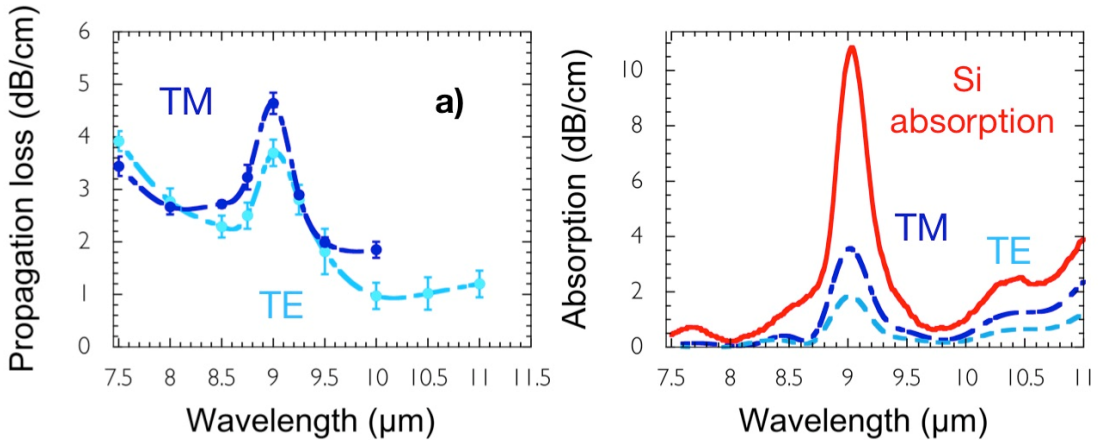

Figure 4: a) Measured waveguide losses in both transverse magnetic (TM) and transverse electric (TE) polarization. b) Measured Si loss shown alongside the Si loss scaled by the modal overlap for the fundamental TE and TM waveguide modes.

The Ge epitaxial layer was removed by selective wet etching in H_2O_2. The reverse side of the Si piece was subsequently polished, and transmission and reflection measurements were taken on a Bruker IFS 66 VS Fourier Transform Infrared (FTIR) spectrometer. The Si loss was subsequently calculated, and has been plotted in dB/cm in Fig 4b). The corresponding waveguide propagation loss (from Si absorption only) is also shown for TE and TM modes. As shown in Fig. 4b), the increased modal overlap with the substrate for TM modes leads to increased optical loss from interstitial oxygen. This is extremely consistent with the observed propagation losses, which confirms and validates the assumption of the loss mechanism. Above 10 µm wavelength, the TM mode could not be measured due to low signal to noise, meaning the loss could not be accurately measured (this is likely due to TM modes being close to cut-off, and the low laser power from the relevant QCL chip). In TE polarization the losses reach as low as ~ 1 dB/cm above 10 µm wavelength; to our knowledge this is the lowest losses demonstrated for a dielectric integrated wavelength at these wavelengths. It is evident, however, that subtracting the Si modal losses leaves a trend of decreasing loss with wavelength. An analytical (Payne and Lacey [36]) scattering model, which has been modified for 3d structures [37], was used to examine the effects of roughness in the MIR. It was found that the slope observed in our waveguide losses could be described by an rms roughness of ~ 20 nm and a correlation length of 150 nm. This, however should only be treated as an approximation as the model is designed for ridge waveguides. This does, however, demonstrate that moderate roughness can still lead to significant loss in the MIR. While the SEM images appear smooth, a detailed atomic force microscopy analysis would be required to confirm if the roughness is likely to lead to significant scattering loss. There are other potential mechanisms that could produce losses; C_4F_8 is used a passivation gas in the etch process that could leave some residue on the waveguide sidewalls. This polymer has absorption lines in the MIR [38]. Misfit and threading dislocations are present at the Ge/Si interface, but do not have any well-known electronic states in the bandgap that cause absorption at the measurement wavelength. Scattering from threading dislocations is thought to be unlikely, as a dislocation density of ~ 1 x 10^7 cm^{-2} equates to 0.1 μm^2. This means that in our 4 µm wide waveguide there is on average 1 thread every 2.5 µm (in the propagation direction). However, this threading dislocation density is measured at the top plane of the Ge and could be substantially larger near the Ge-on-Si interface where threads cross-link and annihilate. This experiment, however, would require more analysis using wafer growths with varying dislocation densities. Finally, in the case of imperfect facets, the assumed reflectivity could be incorrect, and lead to error on the measurement that has not been quantified. This would be most likely to mean that the losses have been overestimated, however, and is not expected to be significant.

6. DISCUSSION

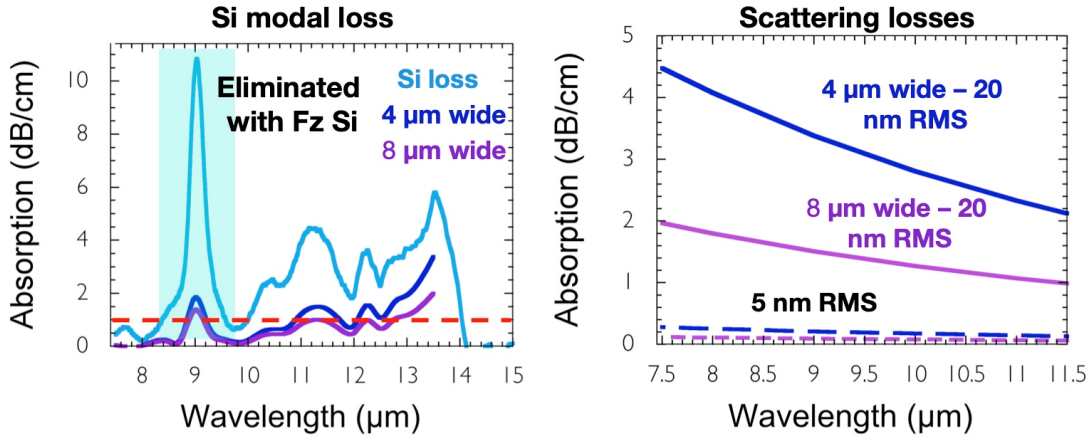

Figure 5: a) Si substrate loss scaled by the modal overlap of 2 µm thick Ge rib waveguides of different widths. The loss of 1 dB/cm has been indicated with a dashed red line. The peak corresponding to an interstitial oxygen bond in Si has been highlighted, which can be nearly fully removed using float-zone Si. b) The calculated scattering losses for waveguides of varying width and RMS roughness. A blue line corresponds to 4 µm wide, while a purple line indicates 8 µm width. The analytical Payne and Lacey model assumes a correlation length of 150 nm.

The observed losses are already encouraging, and verify the potential of Ge-on-Si waveguides > 8.5 μm wavelength. There are also a number of practical means by which the observed losses could be reduced. Firstly, float-zone Si wafers could be used which almost fully eliminates the absorption at 9 μm wavelength due to interstitial oxygen. Altering the waveguide geometry can also reduce the overlap with the Si substrate. While 4 μm wide waveguides were chosen to be single mode across the full measurement range, waveguide widths could be tailored and optimized for different wavelengths of operation. As shown in Fig 5, increasing the width in TE polarization will reduce the Si overlap, bringing the Si contribution to the losses to below 1 dB/cm, when using float zone Si. Likewise, if present, scattering losses can also be addressed by very practical means, including electron beam patterning techniques such as 'multipass', which reduces line edge roughness by writing features multiple times with varying stage offsets. Quantifying the surface roughness will be the subject of future work.

7. CONCLUSION

Record low losses are shown for Ge-on-Si waveguides operating up to 11 μm wavelength. Ge epitaxial layers of 2 μm thickness were grown on (100) Si wafers. SIMs measurements confirmed the background doping density to be below 5×10^{14} cm^{-3}, meaning that free carrier absorption can be ruled out as a mechanism for absorption. The effect of the Si substrate loss is demonstrated for the first time and the measured Si losses from FTIR transmission/reflection are consistent with the observed waveguide propagation losses, when taking into account the modal overlap. The residual losses have been attributed to a scattering process; likely to be from etched sidewalls but possible from the Ge/Si interface. Despite this, losses are found to reach as low as ~ 1 dB/cm at wavelengths ~ 10 μm wavelength. It has been demonstrated that through practical means, losses could be reduced to ~ 1 dB/cm across the full measurement range. These results indicate that the Ge-on-Si platform is well suited to mid-infrared sensing in the 8 – 14 atmospheric transmission window.

REFERENCES

[1] R. Soref, "Mid-infrared photonics in silicon and germanium," Nat. Photonics 4, 495–497 (2010).

[2] L. Baldassarre, E. Sakat, J. Frigerio, A. Samarelli, K. Gallacher, E. Calandrini, G. Isella, D. J. Paul, M. Ortolani, and P. Biagioni, "Midinfrared plasmon-enhanced spectroscopy with germanium antennas on silicon substrates," Nano Lett. 15, 7225–7231 (2015).

[3] L. Rothman, I. Gordon, Y. Babikov, A. Barbe, D. C. Benner, P. Bernath, M. Birk, L. Bizzocchi, V. Boudon, L. Brown, A. Campargue, K. Chance, E. Cohen, L. Coudert, V. Devi, B. Drouin, A. Fayt, J.-M. Flaud, R. Gamache, J. Harrison, J.-M. Hartmann, C. Hill, J. Hodges, D. Jacquemart, A. Jolly, J. Lamouroux, R. L. Roy, G. Li, D. Long, O. Lyulin, C. Mackie, S. Massie, S. Mikhailenko, H. Müller, O. Naumenko, A. Nikitin, J. Orphal, V. Perevalov, A. Perrin, E. Polovtseva, C. Richard, M. Smith, E. Starikova, K. Sung, S. Tashkun, J. Tennyson, G. Toon, V. Tyuterev, and G. Wagner, "The HITRAN2012 molecular spectroscopic database," J. Quant. Spectrosc. Radiat. Transf. 130, 4 – 50 (2013).

[4] J. Chou, Hazardous Gas Monitors: A Practical Guide to Selection, Operation, and Applications (McGraw-Hill, New York, USA, 2000).

[5] P. M. Pellegrino, E. L. Holthoff, and M. E. Farrell, eds., Laser Based Optical Detection of Explosives (CRC, 2017).

[6] E. R. Deutsch, P. Kotidis, N. Zhu, A. K. Goyal, J. Ye, A. Mazurenko, M. Norman, K. Zafiriou, M. Baier, and R. Connors, "Active and passive infrared spectroscopy for the detection of environmental threats," Proc. SPIE 9106, 9106 – 9106 – 10 (2014).

[7] Paolo Biagioni, Jacopo Frigerio, Antonio Samarelli, Kevin Gallacher, Leonetta Baldassarre, Emilie Sakat, Eugenio Calandrini, Ross W. Millar, Valeria Giliberti, Giovanni Isella, Douglas J. Paul, Michele Ortolani, "Group-IV midinfrared plasmonics," J. Nanophoton. 9(1) 093789 (23 February 2015)

[8] Frigerio, J., Ballabio, A., Gallacher, K., Gilberti, V., Baldassarre, L., Millar, R. W., Milazzo, R., Maiolo, L., Minotti, A., Bottegoni, F., Biagioni, P., Paul, D. J., Ortolani, M., Pecora, A., Napolitani, E. & Isella, G. "Optical properties of highly n-doped germanium obtained by in situ doping and laser annealing" J. Phys. D. Appl. Phys. 50, 465103 (2017).

[9] K. Gallacher, A. Ballabio, R. W. Millar, J. Frigerio, A. Bashir, I. MacLaren, G. Isella, M. Ortolani, and D. J. Paul, "Mid-infrared intersubband absorption from p-Ge quantum wells grown on Si substrates," Appl. Phys. Lett. 108, 091114 (2016).

[10] A. I. Yakimov, V. V. Kirienko, A. A. Bloshkin, V. A. Armbrister, A. V. Dvurechenskii, and J.-M. Hartmann, "Photovoltaic Ge/SiGe quantum dot mid-infrared photodetector enhanced by surface plasmons," Opt. Express 25, 25602-25611 (2017)

[11] R. W. Millar, D. C. S. Dumas, K. F. Gallacher, P. Jahandar, C. MacGregor, M. Myronov, and D. J. Paul, "Mid-infrared light emission > 3 μm wavelength from tensile strained GeSn microdisks," Opt. Express 25, 25374–25385 (2017).

[12] J. Margetis, S. Al-Kabi, W. Du, W. Dou, Y. Zhou, T. Pham, P. Grant, S. Ghetmiri, A. Mosleh, B. Li, J. Liu, G. Sun, R. Soref, J. Tolle, M. Mortazavi, and S.-Q. Yu, "Si-Based GeSn lasers with wavelength coverage of 2 - 3 μm and operating temperatures up to 180 K," ACS Photonics 5, 827–833 (2018).

[13] S. Assali, J. Nicolas, S. Mukherjee, A. Dijkstra, and O. Moutanabbir, "Atomically uniform Sn-rich GeSn semiconductors with 3.0-3.5 μ m room-temperature optical emission," Appl. Phys. Lett., vol. 112, no. 25, pp. 1–6, 2018.

[14] Rei Kitamura, Laurent Pilon, and Miroslaw Jonasz, "Optical constants of silica glass from extreme ultraviolet to far infrared at near room temperature," Appl. Opt. 46, 8118-8133 (2007)

[15] J. S. Penadés, A. Sánchez-Postigo, M. Nedeljkovic, A. Ortega-Monux, J. G. Wangüemert-Pérez, Y. Xu, R. Halir, Z. Qu, A. Z. Khokhar, A. Osman, W. Cao, C. G. Littlejohns, P. Cheben, I. Molina-Fernández, and G. Z. Mashanovich, "Suspended silicon waveguides for long-wave infrared wavelengths," Opt. Lett. 43, 795–798 (2018).

[16] M. Sinobad, C. Monat, B. Luther-davies, P. Ma, S. Madden, D. J. Moss, A. Mitchell, D. Allioux, R. Orobtchouk, S. Boutami, J.-M. Hartmann, J.-M. Fedeli, and C. Grillet, "Mid-infrared octave spanning supercontinuum generation to 8.5 μm in silicon-germanium waveguides," Optica 5, 360–366 (2018).

[17] Joan Manel Ramirez, Qiankun Liu, Vladyslav Vakarin, Xavier Le Roux, Jacopo Frigerio, Andrea Ballabio, Carlos Alonso-Ramos, Enrico Talamas Simola, Laurent Vivien, Giovanni Isella, and Delphine Marris-Morini, "Broadband integrated racetrack ring resonators for long-wave infrared photonics," Opt. Lett. 44, 407-410 (2019)

[18] J. M. Ramirez, Q. Liu, V. Vakarin, J. Frigerio, A. Ballabio, X. Le Roux, D. Bouville, L. Vivien, G. Isella, and D. Marris-Morini, "Graded SiGe waveguides with broadband low-loss propagation in the mid infrared," Opt. Express 26, 870-877 (2018)

[19] M. Yang, Y. Guo, J. Wang, Z. Han, K. Wada, L. C. Kimerling, A. M. Agarwal, J. Michel, G. Li, and L. Zhang, "Mid-IR supercontinuum generated in low-dispersion Ge-on-Si waveguides pumped by sub-ps pulses," Opt. Express 25, 16116 (2017)

[20] N. K. Hon, R. Soref, and B. Jalali, "The third-order nonlinear optical coefficients of Si, Ge, and Si1−xGex in the midwave and longwave infrared," J. Appl. Phys. 110, 011301 (2011).

[21] M. Nedeljkovic, J. S. Penadés, C. J. Mitchell, A. Z. Khokhar, S. Stankovic, T. D. Bucio, C. G. Littlejohns, F. Y. Gardes, and G. Z. Mashanovich, "Surface-grating-coupled low-loss Ge-on-Si rib waveguides and multimode interferometers," IEEE Photonic Tech L 27, 1040–1043 (2015).

[22] Y.-C. Chang, V. Paeder, L. Hvozdara, J.-M. Hartmann, and H. P. Herzig, "Low-loss germanium strip waveguides on silicon for the mid-infrared." Opt. Lett. 37, 2883–2885 (2012).

[23] Aditya Malik, Sarvagya Dwivedi, Liesbet Van Landschoot, Muhammad Muneeb, Yosuke Shimura, Guy Lepage, Joris Van Campenhout, Wendy Vanherle, Tinneke Van Opstal, Roger Loo, and Gunther Roelkens, "Ge-on-Si and Ge-on-SOI thermo-optic phase shifters for the mid-infrared," Opt. Express 22, 28479-28488 (2014)

[24] Carlos Alonso-Ramos, Milos Nedeljkovic, Daniel Benedikovic, Jordi Soler Penadés, Callum G. Littlejohns, Ali Z. Khokhar, Diego Pérez-Galacho, Laurent Vivien, Pavel Cheben, and Goran Z. Mashanovich, "Germanium-on-silicon mid-infrared grating couplers with low-reflectivity inverse taper excitation," Opt. Lett. 41, 4324-4327 (2016)

[25] B. Troia, J. S. Penades, A. Z. Khokhar, M. Nedeljkovic, C. Alonso-Ramos, V. M. N. Passaro, and G. Z. Mashanovich, "Germanium-on-silicon vernier-effect photonic microcavities for the mid-infrared," Opt. Lett. 41, 610–613 (2016).

[26] A. Osman, M. Nedeljkovic, J. Soler Penades, Y. Wu, Z. Qu, A. Z. Khokhar, K. Debnath, and G. Z. Mashanovich, "Suspended low-loss germanium waveguides for the longwave infrared," Opt. Lett. 43, 5997-6000 (2018)

[27] M. Nedeljkovic, J. S. Penades, V. Mittal, G. S. Murugan, A. Z. Khokhar, C. Littlejohns, L. G. Carpenter, C. B. E. Gawith, J. S. Wilkinson, and G. Z. Mashanovich, "Germanium-on-silicon waveguides operating at mid-infrared wavelengths up to 8.5 μm," Opt. Express 25, 27431–27441 (2017).

[28] R. C. Newman, "Oxygen diffusion and precipitation in Czochralski silicon," J. Physics: Condens. Matter 12, R335 (2000).

[29] L. Colace, G. Masini, F. Galluzzi, G. Assanto, G. Capellini, L. D. Gaspare, E. Palange, and F. Evangelisti, "Metal-Ge-Si heterostructures for near-infrared light detection," J. Vac. Sci. Technol. B 17, 465–467 (1999).

[30] J. I. Pankove, Optical Processes in Semiconductors (Dover, 1971). 23. R. Newman and W. W. Tyler, "Effect of impurities on free-hole infrared absorption in p-type germanium," Phys. Rev. 105, 885–886 (1957).

[31] M. Nedeljkovic, R. Soref, and G. Z. Mashanovich, "Predictions of free-carrier electroabsorption and electrorefraction in germanium," IEEE Photonics J. 7, 1–14 (2015).

[32] H. B. Briggs and R. C. Fletcher, "New infrared absorption bands in p-type germanium," Phys. Rev. 87, 1130–1131 (1952).

[33] D. K. Schroder, Semiconductor Material and Device Characterization (Wiley Interscience, 2006), 3rd ed.

[34] H. H. Li, "Refractive index of silicon and germanium and its wavelength and temperature derivatives," J. Phys. Chem. Ref. Data 9, 561–658 (1980).

[35] K. Gallacher, R.W. Millar, U. Griškevičiūte, L. Baldassarre, M. Sorel, M. Ortolani, and D. J. Paul, "Low loss Ge-on-Si waveguides operating in the 8–14 μm atmospheric transmission window," Opt. Express 26, 25667-25675 (2018)

[36] F. P. Payne and J. P. R. Lacey, "A theoretical analysis of scattering loss from planar optical waveguides," Opt. Quantum Electron. 26, 977–986 (1994).

[37] D. E. Hagan and A. P. Knights, "Mechanisms for optical loss in SOI waveguides for mid-infrared wavelengths around 2 μm," J .Opt. 19, 025801 (2017).

[38] E. Vasekova, E.A. Drage, K.M. Smith, N.J. Mason, "FTIR spectroscopy and radiative forcing of octafluorocyclobutane and octofluorocyclopentene" Journal of Quantitative Spectroscopy and Radiative Transfer, Volume 102, Issue 3, p. 418-424. (2006)